CONSTRAINING WARM DARK MATTER MASS WITH COSMIC REIONIZATION AND GRAVITATIONAL WAVE

Wei-Wei Tan[1,2], F. Y. Wang[1,2] & K. S. Cheng[3]

[1]School of Astronomy and Space Science, Nanjing University, Nanjing 210093, China, fayinwang@nju.edu.cn
[2]Key laboratory of Modern Astronomy and Astrophysics (Nanjing University), Nanjing 210093, China
[3]Department of Physics, University of Hong Kong, Pokfulam Road, Hong Kong, China
Draft version July 14, 2016

ABSTRACT

We constrain the warm dark matter (WDM) particle mass with the observations of cosmic reionization and CMB optical depth. We suggest that the GWs from stellar mass black holes (BHs) could give a further constraint on WDM particle mass for future observations. The star formation rates (SFRs) of Population I/II (Pop I/II) and Population III (Pop III) stars are also derived. If the metallicity of the universe have been enriched beyond the critical value of $Z_{crit} = 10^{-3.5} Z_\odot$, the star formation shift from Pop III to Pop I/II stars. Our results show that the SFRs are quite dependent on the WDM particle mass, especially at high redshifts. Combing with the reionization history and CMB optical depth derived from the recent *Planck* mission, we find that the current data requires the WDM particle mass in a narrow range of $1 \, keV \lesssim m_x \lesssim 3 \, keV$. Furthermore, we suggest that the stochastic gravitational wave background (SGWB) produced by stellar BHs could give a further constraint on the WDM particle mass for future observations. For $m_x = 3 \, keV$ with Salpeter (Chabrier) initial mass function (IMF), the SGWB from Pop I/II BHs has a peak amplitude of $\Omega_{GW} \approx 2.8 \times 10^{-9}$ (5.0×10^{-9}) at $f = 316 Hz$, while the GW radiation at $f < 10 Hz$ is seriously suppressed. For $m_x = 1 \, keV$, the SGWB peak amplitude is the same as that of $m_x = 1 \, keV$, but a little lower at low frequencies. Therefore, it is hard to constrain the WDM particle mass by the SGWB from Pop I/II BHs. To assess the detectability of GW signal, we also calculate the signal to noise ratio (SNR), which are SNR = 37.7 (66.5) and 27 (47.7) for $m_x = 3 \, keV$ and $m_x = 1 \, keV$ for Einstein Telescope (ET) with Salpeter (Chabrier) IMF, respectively. The SGWB from Pop III BHs is seriously dependent on the WDM particle mass, the GW strength could be an order of magnitude different and the frequency band could be two times different for $m_x = 1 \, keV$ and $m_x = 3 \, keV$. Moreover, the SGWB from Pop III BHs with $m_x = 1 \, keV$ could be detected by LISA for one year of observation, but can not for $m_x = 3 \, keV$.

Subject headings: cosmology: theory - dark matter - cosmology: reionization - gravitational waves

1. INTRODUCTION

The astrophysical and cosmological probes have confirmed that baryons constitute only some 16% of the total matter in the Universe. The rest of the mass is in the form of 'dark matter' (DM). The nature of DM particles is poorly understood, as they do not interact with baryons. Many indirect searches have been carried out, including searching for γ-ray signals at the Galactic center, in nearby galaxies, and the diffuse γ-ray background (Ackermann et al. 2012, 2014; The Fermi LAT collaboration 2015). However, none of them could provide robust evidence for the observation of DM. The GeV γ-ray excess from the Galactic center could be a signal of DM annihilation, but still can not be confirmed (Daylan, Portillo, & Finkbeiner 2015; Zhou et al. 2015).

Among various DM candidates, the most popular candidate is the weakly interacting massive particles (WIMPs; like the neutralino), which have mass in GeV range (Jungman, Kamionkowski, & Griest 1996; Bertone, Hooper, & Silk 2005; Hooper & Profumo 2007; Feng 2010). The WIMPs are non-relativistic at the epoch of decoupling from the interacting particles and have negligible free-streaming velocities. Therefore, they are 'cold', called cold dark matter (CDM). In CDM scenario, 'halos' formed in small clumps, and then merged together into larger and massive objects. Galaxies formed in these halos are because of the cooling of atomic hydrogen (H; Tegmark et al. 1997) or molecular hydrogen (H_2; Ciardi, Ferrara, & Abel 2000; Haiman, Abel, & Rees 2000).

On large cosmological scales (from the range $\sim 1 \, Gpc$ down to $\sim 10 \, Mpc$), CDM paradigm has great success in explaining the observed universe and reproducing the luminous structures (Fixsen et al. 1996; Borgani & Guzzo 2001; Lange et al. 2001; Cole et al. 2005; Tegmark et al. 2006; Benson 2010; Wang 2013; Hinshaw et al. 2013; Slosar et al. 2013; Planck Collaboration et al. 2014; Wei et al. 2016). However, on small scales ($\lesssim 1 \, Mpc$), there are still some discrepancies between the CDM paradigm and observations: (a) the core-cusp problem (Navarro, Frenk, & White 1997; Subramanian, Cen, & Ostriker 2000). CDM simulations predict a cusp-core DM halo, whereas the observations find them cored (Salucci et al. 2012); (b) too big to fail problem (Boylan-Kolchin, Bullock, & Kaplinghat 2012). CDM simulations predict a central DM density significantly higher than the observation that allowed; and (c) the 'missing satellite problem'. N-body simulations based on the CDM paradigm predict a number of sub-halos larger than that of satellites found in our Galaxy (Klypin et al. 1999; Moore et al. 1999; Papastergis et al. 2011). Many methods have been proposed to solve these small scale problems, such as modifying the nature of DM from the CDM paradigm (Hu, Barkana, & Gruzinov 2000; Spergel & Steinhardt 2000; Su & Chen 2011; Menci, Fiore, & Lamastra 2012), adding supernova feedback effect in simulation (Weinberg & Katz 2002; Mashchenko, Couchman, & Wadsley 2006; Governato et al. 2010; Pontzen & Governato 2014), and considering the interplay between DM and baryons during the forma-

tion of the galaxy (El-Zant, Shlosman, & Hoffman 2001; Tonini, Lapi, & Salucci 2006; Pontzen & Governato 2014). However, these methods are insufficient to solve all the above problems.

Alternatively, a more possible solution to these small scale problems is the warm dark matter (WDM) scenario, with DM particle mass in keV range. The candidates are sterile neutrinos (Dodelson & Widrow 1994; Abazajian, Fuller, & Patel 2001; Abazajian & Koushiappas 2006; Shaposhnikov & Tkachev 2006; Boyarsky, Ruchayskiy, & Shaposhnikov 2009; Kusenko 2009; Abazajian et al. 2012) and gravitinos (Kawasaki, Sugiyama, & Yanagida 1997; Gorbunov, Khmelnitsky, & Rubakov 2008). WDM particles are lighter than CDM particles, so they could remain relativistic for longer time in the early universe and retain a non-negligible velocity dispersion. They are more easy to free-stream out from small scale perturbations, and suppress the formation of subhalos (Bode, Ostriker, & Turok 2001; Lovell et al. 2014). The most powerful test for WDM scenario is the high-redshift universe. A number of works have been done to constrain the WDM particle mass (m_x). For example, Kang, Macciò, & Dutton (2013) gave a lower limit of $m_x \gtrsim 0.75\,\text{keV}$ by reproducing the stellar mass functions and Tully-Fisher relation for $0 < z < 3.5$ galaxies. Viel et al. (2013) used Lyman-α flux power spectrum measured from high-resolution spectra of 25 quasars to obtain a lower limit of $m_x \gtrsim 3.3\,\text{keV}$. de Souza et al. (2013) used high-redshift ($z > 4$) gamma-ray bursts to constrain $m_x \gtrsim 1.6 - 1.8\,\text{keV}$. Dayal et al. (2015b) constrained $m_x \gtrsim 2.5\,\text{keV}$ by comparing the semi-analytic merger tree based framework for high-redshift ($z \simeq 5 - 20$) galaxy formation with reionization indicators. Lapi & Danese (2015) gave a narrow constraint of $2 < m_x < 3\,\text{keV}$ by combining the measurements of the galaxy luminosity functions out $z \sim 10$ from *Hubble Space Telescope* (HST) with the reionization history of the universe from the *Planck* mission. Pacucci, Mesinger, & Haiman (2013) constrained $m_x \gtrsim 1\,\text{keV}$ by using the number density of $z \approx 10$ lensed galaxies.

Given that structures are formed hierarchically and WDM scenario smears out the power on small scale, the number density of the smallest halos (or galaxies) at high redshift will be strongly decreased, and then the SFR. Especially the SFRs of Pop III stars and high-redshift Pop I/II stars, because they are firstly formed in these small halos (Barkana & Loeb 2001). Pop III stars are the massive stars with masses $\gtrsim 100 M_\odot$ (e.g., Bromm, Coppi, & Larson 1999; Abel, Bryan, & Norman 2000; Nakamura & Umemura 2001), which are formed in metal-free gas. The deaths of Pop III stars lead to the metal enrichment of intergalactic medium (IGM) via supernova feedback, and subsequently the formation of Pop I/II stars (the cricitical metallicity is $10^{-3.5} Z_\odot$; Ostriker & Gnedin 1996; Madau & Rees 2001; Bromm & Loeb 2003; Furlanetto & Loeb 2003). The mass of Pop I/II stars is in the range of $0.1 \sim 100 M_\odot$. The first light from Pop III stars brought the end of the cosmic dark ages, and then the universe began to reionize. Recent observation from *Planck* mission measured the integrated CMB optical depth with $\tau = 0.066^{+0.013}_{-0.013}$ (with the constraint from *Planck* TT+low polarization+lesing+BAO; Planck Collaboration et al. 2015), and most of the observations show that the universe was fully reionized at redshift $z \simeq 6$ (Chornock et al. 2013;

Treu et al. 2013; Pentericci et al. 2014; Schenker et al. 2014; McGreer, Mesinger, & D'Odorico 2015). These measurements gauge the level of the reionization history from the high-redshift stars. Furthermore, as the high-redshift stars formed in small halos are greatly affected by the halo number density, their formation rates could provide a indirect test on the WDM scenario.

On September 14, 2015 the Advanced LIGO observed the gravitational-wave event GW150914 (Abbott et al. 2016a). The observed signal is consistent with a black-hole binary waveform with the component masses of $m_1 = 36^{+5}_{-4}\,\text{M}_\odot$ and $m_2 = 29^{+4}_{-4}\,\text{M}_\odot$, which demonstrates the existence of stellar-mass black holes massive than $25\,\text{M}_\odot$. The second GW candidate GW 151226 was observed by the twin detectors of the Advanced LIGO on December 26, 2015 (Abbott et al. 2016b). The inferred initial BH masses are $14.2^{+8.3}_{-3.7}\,\text{M}_\odot$ and $7.5^{+2.3}_{-2.3}\,\text{M}_\odot$, and the final BH mass is $20.8^{+6.1}_{-1.7}\,\text{M}_\odot$. The decay of the waveform at the final period are also observed, which are consistent with the damped oscillations of a black hole relaxing to a stationary Kerr configuration. The collapses of Pop I/II or Pop III stars into black holes (BHs) could also release gravitational waves (GWs; Buonanno et al. 2005; Sandick et al. 2006; Suwa et al. 2007; Pereira & Miranda 2010; Ott et al. 2013; Yang, Wang, & Dai 2015), which is dominated by 'quasi-normal ringing' of a perturbed black hole. Therefore, it is expected that the Advanced LIGO could also observe this kind of gravitational wave radiations. In this paper, we will calculate the SGWB from BH 'ringing', which relates with the de-excitation of the BH quasi-normal modes. Because the SGWB is quite dependent on the SFR, it could be used to constrain the WDM particle mass indirectly. Several GW detectors are operating or planed in future: advanced VIRGO and LIGO working at $\approx 10\text{Hz} - 3\text{kHz}$, the Einstein Telescope (ET) with the sensitive frequency of $1 - 100\text{Hz}$, the Laser Interferometer Space Antenna [1] (LISA) covering the frequency range of $10^{-4} - 0.1\text{Hz}$, the Decihertz Interferometer Gravitational wave Observatory[2] (DECIGO)(Kudoh et al. 2006), and the Big Bang Observer (BBO) operating in the range $0.01 - 10$ Hz. Therefore, GW signal from BHs ringing will open a new window for the restriction of the WDM particle mass.

This paper is organized as follows. In section 2, we describe the hierarchical formation scenario in the framework of WDM paradigm. In section 3, we construct the SFRs of Pop I/II and Pop III stars, and compare them with the recent observations. In section 4, we constrain the WDM particle mass with the CMB optical depth and the reionization history. In section 5, we calculate the SGWBs from Pop I/II and Pop III BHs. Finally, conclusion and discussion are given in section 6. Throughout this paper, we adopt the standard flat cosmology with cosmological parameters $\Omega_\Lambda = 0.72$, $\Omega_m = 0.28$, $\Omega_b = 0.046$, $H_0 = 70\,\text{km}\,\text{s}^{-1}\,\text{Mpc}^{-1}$, and $\sigma_8 = 0.82$.

2. HIERARCHICAL FORMATION SCENARIO IN WDM MODEL

In the framework of hierarchical formation scenario, Press & Schechter (1974) first gave a straightforward semi-analytic approach for the abundance of dark matter halos, which is known as the Press-Schechter (PS) formalism. An improved PS-like simulation was proposed by Sheth & Tormen (1999), and they considered the collapse

---

[1] http://lisa.nasa.gov/
[2] http://universe.nasa.gov/program/vision.html

of the ellipsoidal halo rather than the spherical one. In quantitative studies (Greif & Bromm 2006; Heitmann et al. 2006; Reed et al. 2007), the Sheth-Tormen (ST) approach was proved to be more accurate. Therefore, we also choose ST formalism in our following calculations.

Based on the ST formalism, the halo mass function could be described as

$$f_{\rm ST}(\sigma) = A \sqrt{\frac{2a_1}{\pi}} \left[1 + \left(\frac{\sigma^2}{a_1 \delta_{\rm c}^2} \right)^p \right] \frac{\delta_{\rm c}}{\sigma} \exp\left[-\frac{a_1 \delta_{\rm c}^2}{2\sigma^2} \right], \quad (1)$$

where $A = 0.3222$, $a_1 = 0.707$, $p = 0.3$ is the best-fitting values from simulations, $\delta_{\rm c} = 1.686$ is the critical over density, and $\sigma(M, z)$ is the variance of the linear density field. The number of dark matter halos per comoving volume at a given redshift within the mass interval $M \sim M + \mathrm{d}M$ could be related to $f_{\rm ST}$ as

$$\mathrm{d}n_{\rm ST}(M, z) = \frac{\rho_{\rm m}}{M} \frac{\mathrm{d}\ln\sigma^{-1}}{\mathrm{d}M} f_{\rm ST}(\sigma)\mathrm{d}M, \quad (2)$$

where $\rho_{\rm m}$ is the mean density of the universe. In a Gaussian density field, the variance of the linear density field in the local universe with mass M is given by

$$\sigma^2(M, 0) = \frac{1}{2\pi^2} \int_0^\infty k^2 P(k) W^2(kM)\mathrm{d}k, \quad (3)$$

where $P(k)$ is the power spectrum of the density fluctuations at $z = 0$. $W(k, M)$ is the sharp k-space filtering with

$$W(k, M) = \begin{cases} 1, & \text{if } k \leq k_s(R), \\ 0, & \text{if } k > k_s(R), \end{cases} \quad (4)$$

where $R = (3M/4\pi\rho)^{1/3}$ is the radius of the halo with mass M, and $k_{\rm s} = a/R$ with $a = 2.5$ (Benson et al. 2013). The redshift dependence enters only through the linear growth factor $D(z)$, which could be taken as $D(z) = g(z)/[g(0)(1+z)]$ with

$$g(z) \approx \frac{5\Omega_{\rm m}(z)}{2[\Omega_{\rm m}(z)^{4/7} - \Omega_\Lambda(z) + (1 + \frac{\Omega_{\rm m}(z)}{2})(1 + \frac{\Omega_\Lambda(z)}{70})]}, \quad (5)$$

therefore, $\sigma(M, z) = \sigma(M, 0)D(z)$.

In the CDM model, the primordial power spectrum is assumed to be power dependent on scale and multiplied by a transfer function, where the fluctuations are only determined by the interplay between self-gravitation, pressure and damping processes. However, in the WDM model, the WDM particles are relativistic. So the linear fluctuation amplitude is suppressed below the free-streaming scale of the WDM particle. The comoving free-streaming scale is given by (Bode, Ostriker, & Turok 2001)

$$\lambda_{\rm fs} \approx 0.11 \left(\frac{\Omega_{\rm x} h^2}{0.15} \right)^{1/3} \left(\frac{m_{\rm x}}{\rm keV} \right)^{-4/3} \rm Mpc, \quad (6)$$

where $\Omega_{\rm x}$ is the fraction of the energy density in WDM particles relative to the critical energy density, h is the Hubble constant in unites of $100\,\rm km\,s^{-1}\,Mpc^{-1}$, and $m_{\rm x}$ is the WDM particle mass. Following Bode, Ostriker, & Turok (2001), the power spectrum should be modified by a transfer function below the free-streaming scale, which can be described by

$$P_{\rm WDM}(k) = P_{\rm CDM}(k) \left[1 + (\epsilon k)^{2\mu} \right]^{-5\mu}, \quad (7)$$

where $\mu = 1.12$, $P_{\rm WDM}(k)$ and $P_{\rm CDM}(k)$ are the power spectra in WDM and CDM paradigms, respectively. ϵ is related

with both the WDM particle mass $m_{\rm x}$ and the energy density fraction $\Omega_{\rm x}$, which can be written as

$$\epsilon = 0.049 \left(\frac{\Omega_{\rm x}}{0.25} \right)^{0.11} \left(\frac{m_{\rm x}}{\rm keV} \right)^{-1.11} \left(\frac{h}{0.7} \right)^{1.22} h^{-1}\rm Mpc. \quad (8)$$

As mentioned above, the smallest structure formed in WDM model is greatly suppressed by the residual velocity dispersion of WDM particles. Therefore, the minimum halo mass should also be quite dependent on the WDM particle mass. We describe the minimum halo mass as (de Souza et al. 2013)

$$M_{\rm WDM} \approx 1.8 \times 10^{10} \left(\frac{\Omega_{\rm x} h^2}{0.15} \right)^{1/2} \left(\frac{m_{\rm x}}{1\rm keV} \right)^{-4} \rm M_\odot. \quad (9)$$

Then, we could calculate the fraction of the baryons inside structures. Here we assume that the baryon distribution traces the dark matter distribution without bias, and the baryonic density is proportional to the density of dark matter. Therefore, the baryonic fraction in structures can be given by

$$f_{\rm b}(z) = \frac{\int_{M_{\rm min}}^\infty n_{\rm ST}(M, z)M\mathrm{d}M}{\rho_{\rm m}}, \quad (10)$$

where $\rho_{\rm m}$ is the mean density of the universe. Considering that the minimum halo should be capable of forming stars, we rewrite the minimum halo mass as

$$M_{\rm min} = \rm Max[M_{\rm gal}(z), M_{\rm WDM}(m_{\rm x})], \quad (11)$$

where $M_{\rm gal}(z)$ corresponds to the halo mass that could be efficiently cooling by H_2 gas with the virial temperature $T_{\rm vir} = 10^4$ Kelvin, which could be given by

$$M_{\rm gal}(z) \approx 10^8 \times \left(\frac{\eta}{0.6} \right)^{-2/3} \left(\frac{T_{\rm vir}}{10^4\rm K} \right)^{3/2} \left(\frac{1+z}{10} \right)^{-3/2} \rm M_\odot, \quad (12)$$

here $\eta = 1.22$ is the mean molecular weight. In fact, $M_{\rm WDM} > M_{\rm gal}$ for $m_{\rm x} < 2\,\rm keV$, and hence $M_{\rm min}$ is not sensitive to the exact value of $M_{\rm gal}$ for low WDM particle mass.

The baryonic fraction in structures can be given by equation (10), therefore, we could describe the accretion rate of baryon into structures at different cosmic time. Following Daigne et al. (2006), it could be described as

$$a_{\rm b}(t) = \Omega_{\rm b}\rho_{\rm c} \left(\frac{\mathrm{d}t}{\mathrm{d}z} \right)^{-1} \left| \frac{\mathrm{d}f_{\rm b}(z)}{\mathrm{d}z} \right|, \quad (13)$$

where $\rho_{\rm c}$ is the critical density of the universe. The age of the universe could be related to the redshift by

$$\frac{\mathrm{d}t}{\mathrm{d}z} = \frac{9.78h^{-1}\rm Gyr}{(1+z)\sqrt{\Omega_\Lambda + \Omega_{\rm m}(1+z)^3}}. \quad (14)$$

Thereafter, we will calculate the formation rates of Pop I/II and Pop III stars in the framework of WDM paradigm, and study the effect of the WDM particle mass on their formation rates.

3. COSMIC STAR FORMATION RATE

First, we should make it clear that how the matter transfer among stars, interstellar medium (ISM) and intergalactic medium (IGM). Four fundamental processes should be included: (a) the accretion of baryons from IGM to form structures, $a_{\rm b}(t)$; (b) the transfer of baryons from structures

(or ISM) into stars, $\Psi(t)$; (c) stars return mass to the ISM through stellar winds and supernovae, $M_{ej}(t)$; (d) the outflow of baryons from structures into IGM through galactic winds and direct ejecta of stellar supernova, $o(t)$. In this section, we will describe how to calculate the above four processes. For the first point, the baryonic accretion rate $a_b(t)$ is described by equation (13). For the second point, we will calculate both the formation rates of Pop I/II and Pop III stars. For simplicity, we assume both the SFRs follow the Schmidt law (Schmidt 1959, 1963), i.e., SFRs are proportional to the gas density $\rho_g(t)$ in structures. Here we employ an exponentially decreasing SFR for Pop I/II stars, which fits the observational data quite well (Daigne et al. 2006). Hence, we take

$$\Psi_{I/II}(t) = f_1 \frac{\rho_g(t)}{\tau_1} e^{-(t-t_{init})/\tau_1}(1 - e^{-Z_{IGM}/Z_{crit}}), \quad (15)$$

where t_{init} is the initial age of the universe at redshift z_{init} and τ_1 is the star formation time scale. Here we consider $f_1 e^{-(t-t_{init})/\tau_1}$ as the star formation efficiency of Pop I/II stars, which could be determinated by the observed SFR at low redshift. The last term represents the fraction of gas that are metal populated by outflows of structures, where Z_{IGM} is the metallicity of IGM and $Z_{crit} = 10^{-3.5}Z_\odot$ is the critical metallicity. For Pop III stars, we assume an exponential decease star formation model, which could be described as (Daigne 2006)

$$\Psi_{III}(t) = f_2 \rho_g(t) e^{-Z_{IGM}/Z_{crit}}. \quad (16)$$

For the star formation efficiency, we set a typical value of $f_2 = 4.5\%$ (Daigne et al. 2004). Such a value is just located within its theoretically-expected range of $\sim 10^{-6} - 10^{-3}$ (Greif & Bromm 2006; Marassi, Schneider, & Ferrari 2009). Therefore, the total mass rate that goes into stars is

$$\frac{d^2 M_\star}{dVdt} = \Psi_{I/II}(t) + \Psi_{III}(t), \quad (17)$$

which is the sum formation rate of Pop I/II and Pop III stars.

We assume two IMFs for both Pop I/II and Pop III stars. The Salpeter IMF (SIMF; Salpeter 1955) is

$$\Phi(m) \propto m^{-(1+x)}, \quad (18)$$

with $x = 1.35$. The Chabrier IMF (CIMF; Chabrier 2003) is

$$\Phi(m) \propto \begin{cases} \frac{0.158}{m}\exp\frac{[-\log(m/M_\odot)-\log(0.08)]^2}{2\times(0.69)^2}, & \text{if } m \leq 1\,M_\odot, \\ m^{-2.3}, & \text{if } m > 1\,M_\odot, \end{cases} \quad (19)$$

The two IMFs are normalized independently for these two kind of stars, but with different integrate mass range. We consider $m_{inf} = 0.1M_\odot$ and $m_{sup} = 100M_\odot$ for Pop I/II stars, $m'_{inf} = 100M_\odot$ and $m'_{sup} = 500M_\odot$ for Pop III stars.

For the third point, the mass ejected from stars through stellar winds and supernovae into ISM is given by

$$\frac{d^2 M_{ej}}{dVdt} = \int_{m(t)}^{M_{sup}} (m - m_r)\Phi(m)\Psi_{I/II}(t - \tau_m)dm +$$
$$\int_{m'(t)}^{M'_{sup}} (m' - m'_r)\Phi(m')\Psi_{III}(t - \tau_{m'})dm', \quad (20)$$

where $m(t)$ corresponds to the stellar mass whose lifetime is equal to the age of the universe (t). We use the mass-lifetime relation proposed by Scalo (1986) and Copi (1997) to derive $m(t)$ or the stellar lifetime τ_m. The mass remnant m_r depends

on the mass of progenitor, and we give a description for m_r as follows (Pereira & Miranda 2010):

a) Stars with $m < 1\,M_\odot$ do not contribute to M_{ej};

b) Stars with $1\,M_\odot \leq m \leq 8\,M_\odot$ dies as the carbon-oxygen white dwarfs with remnants

$$m_r = 0.1156\,m + 0.4551; \quad (21)$$

c) Stars with $8\,M_\odot < m \leq 10\,M_\odot$ left the oxygen-neon-magnesium white dwarfs as the remnants with $m_r = 1.35\,M_\odot$;

d) Stars with $10\,M_\odot < m < 25\,M_\odot$ left neutron stars as remnants ($m_r = 1.4\,M_\odot$);

e) Stars with $25\,M_\odot \leq m \leq 140\,M_\odot$ produce black hole remnants equal to the helium core before collapse with (see Heger & Woosley 2002),

$$m_r = m_{He} = \frac{13}{24}(m - 20\,M_\odot). \quad (22)$$

f) Stars with $140\,M_\odot \leq m \leq 260\,M_\odot$ explode as pair-instability supernova (PISN) (Heger & Woosley 2002)) and left nothing.

g) Stars with $260\,M_\odot \leq m \leq 500\,M_\odot$ collapse directly into BHs without mass lose.

For the fourth point, the outflow of baryons from structures into the IGM could be computed by

$$o(t) = \frac{2\epsilon}{v_{esc}^2(z)} \int_{\max[8\,M_\odot, m_d(t)]}^{m_{sup}} dm\Phi(m)\Psi_{I/II}[t - \tau(m)]E_{kin}(m) +$$
$$\frac{2\epsilon}{v_{esc}^2(z)} \int_{\max[100\,M_\odot, m'_d(t)]}^{m'_{sup}} dm'\Phi(m')\Psi_{III}[t - \tau(m')]E'_{kin}(m'), (23)$$

where E_{kin} is the kinetic energy released by the explosion of a star with mass m, we give a value of $E_{kin} = 10^{51}$ erg for Pop I/II stars and $E'_{kin} = 10^{52}$ erg for Pop III stars. $\epsilon = 10^{-3}$ is the fraction of kinetic energy that is available to power the outflow. $v_{esc}^2(z)$ is the mean square of the escape velocity of structures at redshift z (e.g., Scully et al. 1997), which cold be described by

$$v_{esc}^2(z) = \frac{\int_{M_{min}}^\infty dM n_{ST}(M, z)M(2GM/R)}{\int_{M_{min}}^\infty dM n_{ST}(M, z)M} \quad (24)$$

Combing equations (13), (17), (20) and (23), we could derive the evolution of the gas density $\rho_g(t)$ in structures at each cosmic time, which could be written as

$$\dot{\rho}_g = -\frac{d^2 M_\star}{dVdt} + \frac{d^2 M_{ej}}{dVdt} + a_b(t) - o(t), \quad (25)$$

and the metal enrichment history of the IGM could be described by

$$Z_{IGM}(t) = \frac{\int_t^{t(z_{ini})} o(t)dt}{\rho_c\Omega_b - \int_t^{t(z_{ini})} a_b(t)dt + \int_t^{t(z_{ini})} o(t)dt}, \quad (26)$$

which is the mass fraction of metal populated gas to IGM gas. Here we assume that stars begin to form at the initial refshift of $z_{ini} = 30$. For Pop I/II stars, we derive τ_1 by comparing the model-predict SFR with the observation from Madau & Dickinson (2014). We find that $\tau_1 = 3.8$ Gyr could reproduce the low-redshift SFR quite well ($z \lesssim 4$), and we derive $f_1 = 0.83$ by normalizing the local SFR to $0.016\,M_\odot$ yr^{-1} Mpc^{-3}. Therefore, the star formation efficiency of Pop I/II stars (or the efficiency of conversion of baryons in the halo to Pop I/II stars) is $0.83\,e^{-(t-t_{init})/(3.8Gyr)}$,

which is consistent with the results from the abundance matching techniques or the gravitational lensing measurements at $z \lesssim 4$ (Mandelbaum et al. 2006; Shankar et al. 2006; Moster, Naab, & White 2013; Velander et al. 2014).

In Figure 1, we show the SFRs obtained from the self-consistency model with different WDM particle masses for Pop I/II and Pop III stars: $m_x = 1\,\mathrm{keV}$ (black solid lines for SIMF, black dashed lines for CIMF), $m_x = 2\,\mathrm{keV}$ (blue solid lines for SIMF, blue dashed lines for CIMF) and $m_x = 3\,\mathrm{keV}$ (red solid lines for SIMF, red dashed lines for CIMF). The observed SFR is taken from Madau & Dickinson (2014). Our model could reproduce the observed SFR at low redshift. The high-redshift SFR varies significantly, and it is sensitive to the WDM particle mass. Especially for Pop III stars, the peak SFR could be orders of magnitude different. Comparing with the observations, we could give a crude constraint on the WDM particle mass. The WDM particle mass should be larger than 1 keV, because the model is insufficient to reproduce the current observation of SFR at redshift $z \gtrsim 5$. In order to test the validation of our model and the parameters involved, we compared our SFRs with the one derived from UV luminosity functions, e.g., SFRs from Robertson et al. (2015) (shown as the gray lines in Figure 1), and the results are comparable for $1\,\mathrm{keV} \lesssim m_x \lesssim 3\,\mathrm{keV}$ at $z \lesssim 10$. On the other hand, we calculated the SFRs by assuming that the SFR (in units of $\mathrm{M_\odot\,yr^{-1}}$) in a structure is directly connected to the halo mass (M_h), which is SFR $\propto M_h^\alpha$. We find that a value of $\alpha = 0.9$ could give the good predictions for SFRs at $3 < z < 9$ for all m_x (shown as the dash-dotted lines in Figure 1), which is also consistent with results derived from the abundance matching techniques (e.g., Shankar et al. 2006; Moster, Naab, & White 2013; Aversa et al. 2015). Furthermore, the transition from Pop III stars to Pop I/II stars is quite different, which is mainly determined by the metal enrichment history. As shown in Figure 2, we calculated the metal enrichment history of IGM for different WDM particle masses (solid lines for SIMF and dashed lines for CIMF). The transition occurs at $z = 10$ for $m_x = 1\,\mathrm{keV}$, $z = 14$ for $m_x = 2\,\mathrm{keV}$ and $z = 17$ for $m_x = 3\,\mathrm{keV}$, which is consistent with the previous results (e.g., Yang, Wang, & Dai 2015). Considering that the transition should not occur at a too much high redshift and the metallicity of IGM should not exceed $Z_\odot$ (Daigne et al. 2006), it seems that the WDM particle mass should less than 3 keV.

4. COSMIC REIONIZATION

The cosmic reionization history is dependent on the high-redshift SFR, meanwhile the high-redshift SFR is sensitively dependent on the WDM particle mass. So the cosmic reionization history could be a useful tool to probe the WDM particle mass. We assume that the cosmic reionization is dominated by the high-redshift stars. Using the SFR derived in the above section, we calculate the rate of ionizing ultraviolet photons escaping from stars into IGM, which reads

$$\dot{n}_\gamma(z) = (1+z)^3 \left(\frac{\Psi(z)_{\mathrm{I/II}}}{m_B} N_\gamma^{\mathrm{I/II}} f_{\mathrm{esc}}^{\mathrm{I/II}} + \frac{\Psi(z)_{\mathrm{III}}}{m_B} N_\gamma^{\mathrm{III}} f_{\mathrm{esc}}^{\mathrm{III}} \right), \quad (27)$$

where $(1+z)^3$ accounts for the conversion of the comoving density into the proper density, $\Psi(z)$ is the SFR, m_B is the baryon mass, N_γ are the number of ionizing UV photons released per baryon, and f_{esc} are the escape fractions of these photons from stars into IGM. Here we take the escape fraction as the constant with $f_{\mathrm{esc}}^{\mathrm{I/II}} = 0.2$, $N_\gamma^{\mathrm{I/II}} = 4000$, $f_{\mathrm{esc}}^{\mathrm{III}} = 0.7$, and $N_\gamma^{\mathrm{III}} = 9 \times 10^4$ (Greif & Bromm 2006). For another

point, many works have shown that the escape fraction should evolve with redshift. Following Hayes et al. (2011), the redshift evolution of f_{esc} could be described by

$$f_{\mathrm{esc}}(z) = \begin{cases} \left(\frac{1+z}{12.1}\right)^{2.57}, & \text{if } z \leq 11.1, \\ 1, & \text{if } z > 11.1. \end{cases} \quad (28)$$

By defining the volume filling fraction of ionized hydrogen $Q_{\mathrm{H_{II}}}$, we could calculate it from the differential equation (e.g., Barkana & Loeb 2001; Wang 2013; Robertson et al. 2013, 2015).

$$\dot{Q}_{\mathrm{H_{II}}} = \frac{\dot{n}_\gamma(z)}{(1+y)n_H(z)} - \alpha_B C(z)(1+y)n_H(z)Q_{\mathrm{H_{II}}}, \quad (29)$$

where $n_H(z) = 1.9 \times 10^{-7}(1+z)^3$ cm^{-3} is the number density of hydrogen, and $\alpha_B = 2.6 \times 10^{-13}$ cm^3 s^{-1} is the recombination coefficient for electron with temperature at about $10^4 K$. The factor y is introduced by considering the ionization of helium, because the universe at the reionization epoch includes both hydrogen and helium, whose mass fractions are $X = 0.74$ and $Y = 0.26$ (Pagel 2000), respectively. Here we assume that the helium was only once ionized, therefore, we derive $y = Y/(4X) \approx 0.08$. The clumping factor of the ionized gas is defined by $C \equiv \langle n_{\mathrm{H_{II}}}^2 \rangle / \langle n_{\mathrm{H_{II}}} \rangle^2 = 2.9$ (e.g., Pawlik, Schaye, & van Scherpenzeel 2009; Shull et al. 2012).

Combing equations (27) and (29), we could give a numerical solution for $Q_{\mathrm{H_{II}}}(z)$ by setting $Q_{\mathrm{H_{II}}} = 0$ at the initial refshift of $z_{\mathrm{ini}} = 30$. Therefore, the CMB optical depth can be calculated by integrating the electron density times the Thomson cross section along proper length as

$$\tau = -(1+y)\sigma_T c \int_0^{z_{\mathrm{ini}}} n_H(z) Q_{\mathrm{H_{II}}}(z) \frac{\mathrm{d}t}{\mathrm{d}z} \mathrm{d}z. \quad (30)$$

Here, the upper limit of the integral value is $z_{\mathrm{ini}} \sim 30$, because the CMB optical depth could be mainly contributed by the electrons at relatively low redshift with $z \ll z_{\mathrm{ini}}$ (Larson et al. 2011).

Observation on the ionization fraction $Q_{\mathrm{H_{II}}}$ is making great progress: the star-forming galaxies showing Lyα emission up to $z \sim 7 - 8$ (Treu et al. 2013; Pentericci et al. 2014; Schenker et al. 2014); the Lyα damping wing absorption constrains from GRB host galaxies (Chornock et al. 2013); the number of dark pixels in Lyα forest observation of background quasars (McGreer, Mesinger, & D'Odorico 2015). Most of the observations give strong evidence that the reionization ending rapidly near $z \simeq 6$. Figure 3 shows the neutral fraction of $1 - Q_{\mathrm{H_{II}}}$ from observations and constrains from SFRs shown in Figure 1. The corresponding CMB optical depth are shown in Figure 4. Comparing with these observations, we could give a robust constraint on the SFR, and hence on WDM particle mass. For constant f_{esc}, the neutral fraction of $1 - Q_{\mathrm{H_{II}}}$ and the CMB optical depth τ are shown in the left panel of Figure 3 and top panel Figure 4, respectively. For $m_x = 1\,\mathrm{keV}$, the reionization photons are mainly contributed by Pop III stars at $z \gtrsim 7.5$ and recombination begin to dominate at $6 \lesssim z \lesssim 7.5$ until Pop I/II stars dominate the reionization at $z \lesssim 6$. The reionization ended at $z \simeq 5.5$. The neutral fraction could fit the observation at $z \lesssim 7$ but much lower for $z \gtrsim 7$. For $m_x = 2\,\mathrm{keV}$, the reionization dominate by Pop III stars at $z \gtrsim 10$, and Pop I/II stars dominate the reionization at $z \lesssim 10$ with the fully reionized epoch at $z \simeq 6.3$, which fits the observation quite well. For $m_x = 3\,\mathrm{keV}$, Pop III stars con-

tribute little photons to the reionization at low redshifts and Pop I/II stars dominate the reionization at $z \lesssim 12$, the reionization ended at $z \simeq 7$. However, this is a little farfetched to the observation. Therefore, it produces too much reionization photons at redshift $z \gtrsim 7$ for $m_x \lesssim 1$ keV or $m_x \gtrsim 3$ keV, which can not fit the observations. For the CMB optical depth of τ, they all located in the range of the measurement from *Planck* (Planck Collaboration et al. 2015). For the evolving f_{esc}, the natural fraction of $1-Q_{H_{II}}$ and τ are shown in the right panel of Figure 3 and bottom panel Figure 4, respectively. The reionization process is faster than that of the constant f_{esc}, because more reionization photons are escaped into IGM. The results show that only a narrow range of 1 keV $< m_x < 2$ keV could fit the observations of $1 - Q_{H_{II}}$ and τ. For $m_x = 3$ keV, neither the neutral fraction nor the CMB optical depth could fit the observations.

5. SGWB FROM BH 'RINGING'

In this section, we will calculate the SGWB from 'ringing' BHs, which are quite dependent on the SFRs of Pop I/II and Pop III stars. The total GW flux received on earth could be written as

$$F_\nu(\nu_{obs}) = \int \frac{1}{4\pi d_L^2} \frac{dE_{GW}}{d\nu} \frac{d\nu}{d\nu_{obs}} \Psi(z)\Phi(m)dmdV, \quad (31)$$

where d_L is the luminosity distance, $dE_{GW}/d\nu$ is the GW energy spectrum of an individual source, $\Psi(z)$ is the SFR, $\Phi(m)$ is the IMF as shown in equation (18) and (19). dV is the comoving volume element. In the above equation, the observed GW energy flux per unit frequency for an individual source is

$$f_\nu(\nu_{obs}) = \frac{1}{4\pi d_L^2} \frac{dE_{GW}}{d\nu} \frac{d\nu}{d\nu_{obs}}, \quad (32)$$

which could also be written as (Carr 1980)

$$f_\nu(\nu_{obs}) = \frac{\pi c^3}{2G} h_{BH}^2, \quad (33)$$

where h_{BH} is the dimensionless GW amplitude produced by a star collapses into a BH. The total GW flux received on earth could also be written as

$$F_\nu(\nu_{obs}) = \frac{\pi c^3}{2G} h_{BG}^2 \nu_{obs}. \quad (34)$$

Combing with the above equations, we obtain

$$h_{BG}^2 = \frac{1}{\nu_{obs}} \int h_{BH}^2 \Psi(z)\Phi(m)dmdV. \quad (35)$$

Following Thorne (1987), the dimensionless amplitude for a star collapses into to a BH with mass m_r is given by

$$h_{BH} \simeq 7.4 \times 10^{-20} \epsilon_{GW}^{1/2} \left(\frac{m_r}{M_\odot}\right)\left(\frac{d_L}{1\ \text{Mpc}}\right)^{-1}, \quad (36)$$

where $\epsilon_{GW} \lesssim 7 \times 10^{-4}$ is the GW radiation efficiency. The corresponding GW frequency in the observer frame is

$$\nu_{obs} \simeq 1.3 \times 10^4 \text{Hz}\left(\frac{M_\odot}{m_r}\right)(1+z)^{-1}, \quad (37)$$

where $(1+z)^{-1}$ accounts for the redshift effect. It is obvious that the observed GW frequency is quite dependent on the BH mass. The maximum BH remnant for Pop I/II stars is $43.3\,M_\odot$, whereas $500\,M_\odot$ for Pop III stars

(Pereira & Miranda 2010). Therefore, the minimum GW frequency would be 12 times lower for Pop III BHs (considering the no time delay between the formation of Pop I/II and Pop III stars).

Usually, the SGWB is described by the dimensionless energy density parameter $\Omega_{GW}(\nu_{obs})$, which is the present GW energy density per logarithmic frequency interval divided by the critical energy density of the present universe ($\rho_c c^2$) (Phinney 2001)

$$\Omega_{GW}(\nu_{obs}) = \frac{1}{\rho_c c^2} \frac{d\rho_{gw}}{d \ln\nu_{obs}}, \quad (38)$$

where ρ_{gw} is the GW energy density, and $\rho_c = 3H_0^2/8\pi G$ is the critical density of the universe. For the astrophysical origin of the SGWBs, $\Omega_{GW}(\nu_{obs})$ could be written as

$$\Omega_{GW}(\nu_{obs}) = \frac{\nu_{obs}}{\rho_c c^3} F_{\nu_{obs}}(\nu_{obs}) = \frac{4\pi^2}{3H_0^2} \nu_{obs}^2 h_{BG}^2. \quad (39)$$

To evaluate the detectability of the GW signal, we also calculated the signal to nose (SNR) for a pair interferometers (e.g., Christensen 1992; Flanagan 1993; de Araujo & Miranda 2005; Regimbau & de Freitas Pacheco 2006),

$$(S/N)^2 = \frac{9H_0^4}{50\pi^4} T \int_0^\infty d\nu \frac{\gamma^2(\nu)\Omega_{GW}^2(\nu)}{\nu^6 S_h^{(1)} S_h^{(2)}}, \quad (40)$$

where $T = 1$ yr is the observation time period, $S_h^{(i)}$ is the spectral noise density, and $\gamma(\nu)$ is the overlap reduction function. For a simple consideration, we assume $S_h^{(1)} = S_h^{(2)}$ and $\gamma = 1$ in our calculation.

Figure 5 shows the SGWBs from Pop I/II and Pop III BHs. The sensitivity of GW detectors are also shown, where one year of observation are assumed (Abadie et al. 2010; Hild et al. 2011; Thrane & Romano 2013). In our calculation, three WDM particle masses with $m_x = 1$ keV, $m_x = 2$ keV and $m_x = 3$ keV are considered. For Pop I/II BHs, the SGWB peaks at $\nu = 316$Hz with the amplitude $\Omega_{GW} = 2.8 \times 10^{-9}$ (5.0×10^{-9}) for SIMF (CIMF), which is above the delectability of ET. The SGWBs from Pop I/II BHs are nearly the same for these three WDM particle masses, with only little difference at lower frequencies. We also calculated the the SNR, which are SNR = 27 (47.7), 34.2 (60.5) and 37.7 (66.5) for $m_x = 1$ keV, $m_x = 2$ keV and $m_x = 3$ keV for ET with SIMF (CIMF), respectively. Therefore, it is impossible to constrain the WDM particle mass with SGWB from Pop I/II BHs. For Pop III BHs, the SGWB shifts to lower frequencies, and the amplitudes are much lower than Pop I/II BHs. The lack of GW radiation at frequency ~ 10 Hz is because stars within mass range of $140 - 260\,M_\odot$ explode as pair-instability supernovae without leaving BHs. Moreover, the SGWB amplitude with $m_x = 1$ keV is nearly an order of magnitude higher comparing with $m_x = 3$ keV, and the peaks shift to lower frequencies. The most interesting result is that the SGWB from Pop III BHs with $m_x = 1$ keV is detectable for LISA, and the SNR is 1.76 (1.7) for SIMF (CIMF). However, it could not be detected for $m_x = 3$ keV, because the SNR is only 0.35(0.33). On the other hand, if LISA detects the SGWB from Pop III BHs, it will be acceptable for $m_x = 1$ keV. However, if LISA will not detect the SGWB from Pop III BHs, the value of $m_x = 1$ keV could be excluded. Therefore, we suggest that the SGWB from Pop III BHs could be another useful tool to constrain the WDM

particle mass.

6. CONCLUSION AND DISCUSSION

Although the CDM paradigm has great success in explaining the large scale structure of the universe, it still have some problems on small scales. An alternatively WDM paradigm could ease these problems by employing the keV WDM particles. In this paper, we calculate the SFRs of Pop I/II and Pop III stars in the framework of WDM paradigm. By using a self-consistent method, we reproduce the SFR at low redshift. We find that the high-redshift SFR is sensitively dependent on the WDM particle mass, especially for Pop III stars. By comparing the model-predicted SFR with the observation, we constrain the WDM particle mass with $m_x > 1$ keV, shown as the black lines in Figure 1. We also calculated the metal enrichment history of IGM, and the transition from Pop III to Pop I/II stars is consistent with the previous results (e.g., Yang, Wang, & Dai 2015), e.g., from $z \sim 10 - 17$ for $m_x \sim 1 - 3$ keV. By considering that the metallicity of IGM does not exceed $Z_\odot$, the WDM particle mass should less than 3 keV.

Combing with the CMB optical depth from *Planck* with $\tau = 0.066^{+0.013}_{-0.013}$ and the ionization fraction $Q_{H_{II}}$ from recent observations, we found that the the WDM particle mass should in the range of 1 keV $\lesssim m_x \lesssim 3$ keV, where we have assumed a constant escape fraction of ionizing photons (e.g., Schultz et al. 2014; Dayal, Mesinger, & Pacucci 2015a). However, many works suggest that the escape fraction should be redshift dependent (e.g., Siana et al. 2010; Blanc et al. 2011; Hayes et al. 2011; Kuhlen & Faucher-Giguère 2012; Dijkstra et al. 2014). By considering an evolving escape fraction, we found a more tight constraint 1 keV $< m_x < 2$ keV.

Finally, recent observation of GW150914 and GW151226 inspires a great interest in the field of GW. Therefore, we cal-

culated the SGWBs form Pop I/II and Pop III BHs. Our results show that the SGWB from Pop I/II BHs is not sensitive to the WDM particle mass, and it could be detected by the ET telescope. However, it is impossible to constrain the WDM particle mass by the SGWB from Pop I/II BHs, because they show little difference for different m_x. For Pop III stars, the SGWB is quite dependent on the WMD particle mass. The peak SGWB amplitude with $m_x = 1$ keV is an order of magnitude higher than $m_x = 3$ keV. The corresponding SNR are 1.76 (1.7) and 0.33 (0.35) for SIMF (CIMF), respectively, which is distinguishable for LISA. Moreover, the SGWBs are derived by assuming a maximum GW generation efficiency of $\epsilon_{GW} = 7 \times 10^{-4}$. Combing with the ET observation of SGWB from Pop I/II BHs, we could give a constraint on ϵ_{GW}. Therefore, a further constraint of m_x (or Pop III SFR) could be given by the observation of LISA. On the other hand, the SGWB from Pop III BHs is also quite dependent on the star formation efficiency of f_2. Therefore, a lower efficiency of f_2 will make it hard to constrain the WDM particle mass by the observation of LISA. Anyway, the large difference of SGWBs from Pop III BHs for different m_x will make it possible to constrain the WDM particle mass in future.

REFERENCES

Abadie J., et al., 2010, CQGra, 27, 173001
Abazajian K. N., et al., 2012, arXiv, arXiv:1204.5379
Abazajian K., Fuller G. M., Patel M., 2001, PhRvD, 64, 023501
Abazajian K., Koushiappas S. M., 2006, PhRvD, 74, 023527
Abbott, B. P., et al., 2016a, PhRvL, 116, 061102
Abbott B. P., et al., 2016b, PhRvL, 116, 241103
Abel T., Bryan G. L., Norman M. L., 2000, ApJ, 540, 39
Ackermann M., et al., 2012, ApJ, 761, 91
Ackermann M., et al., 2014, PhRvD, 89, 042001
Aversa R., Lapi A., de Zotti G., Shankar F., Danese L., 2015, ApJ, 810, 74
Barkana R., Loeb A., 2001, PhR, 349, 125
Benson A. J., 2010, PhR, 495, 33
Benson A. J., et al., 2013, MNRAS, 428, 1774
Bertone G., Hooper D., Silk J., 2005, PhR, 405, 279
Blanc G. A., et al., 2011, ApJ, 736, 31
Bode P., Ostriker J. P., Turok N., 2001, ApJ, 556, 93
Borgani S., Guzzo L., 2001, Natur, 409, 39
Boyarsky A., Ruchayskiy O., Shaposhnikov M., 2009, ARNPS, 59, 191
Boylan-Kolchin M., Bullock J. S., Kaplinghat M., 2012, MNRAS, 422, 1203
Bromm V., Coppi P. S., Larson R. B., 1999, ApJ, 527, L5
Bromm V., Loeb A., 2003, Natur, 425, 812
Buonanno A., Sigl G., Raffelt G. G., Janka H.-T., Müller E., 2005, PhRvD, 72, 084001
Carr B. J., 1980, A&A, 89, 6
Chabrier G., 2003, PASP, 115, 763
Chornock R., Berger E., Fox D. B., Lunnan R., Drout M. R., Fong W.-f., Laskar T., Roth K. C., 2013, ApJ, 774, 26
Christensen N., 1992, PhRvD, 46, 5250
Ciardi B., Ferrara A., Abel T., 2000, ApJ, 533, 594
Cole S., et al., 2005, MNRAS, 362, 505
Copi C. J., 1997, ApJ, 487, 704
Daigne F., Olive K. A., Silk J., Stoehr F., Vangioni E., 2006, ApJ, 647, 773

Daigne F., Olive K. A., Vangioni-Flam E., Silk J., Audouze J., 2004, ApJ, 617, 693
Dayal P., Mesinger A., Pacucci F., 2015a, ApJ, 806, 67
Dayal P., Choudhury T. R., Bromm V., Pacucci F., 2015b, arXiv, arXiv:1501.02823
Daylan T., Portillo S. K. N., Finkbeiner D. P., 2015, AAS, 225, #255.19
de Araujo J. C., Miranda O. D., 2005, PhRvD, 71, 127503
de Souza R. S., Mesinger A., Ferrara A., Haiman Z., Perna R., Yoshida N., 2013, MNRAS, 432, 3218
Dijkstra M., Wyithe S., Haiman Z., Mesinger A., Pentericci L., 2014, MNRAS, 440, 3309
Dodelson S., Widrow L. M., 1994, PhRvL, 72, 17
El-Zant A., Shlosman I., Hoffman Y., 2001, ApJ, 560, 636
Feng J. L., 2010, ARA&A, 48, 495
Fixsen D. J., Cheng E. S., Gales J. M., Mather J. C., Shafer R. A., Wright E. L., 1996, ApJ, 473, 576
Flanagan E. E., 1993, PhRvD, 48, 2389
Furlanetto S. R., Loeb A., 2003, ApJ, 588, 18
Gorbunov D., Khmelnitsky A., Rubakov V., 2008, JHEP, 12, 055
Governato F., et al., 2010, Natur, 463, 203
Greif T. H., Bromm V., 2006, MNRAS, 373, 128
Haiman Z., Abel T., Rees M. J., 2000, ApJ, 534, 11
Hayes M., Schaerer D., Östlin G., Mas-Hesse J. M., Atek H., Kunth D., 2011, ApJ, 730, 8
Heger A., Woosley S. E., 2002, ApJ, 567, 532
Heitmann K., Lukić Z., Habib S., Ricker P. M., 2006, ApJ, 642, L85
Hild S., et al., 2011, CQGra, 28, 094013
Hinshaw G., et al., 2013, ApJS, 208, 19
Hooper D., Profumo S., 2007, PhR, 453, 29
Hu W., Barkana R., Gruzinov A., 2000, PhRvL, 85, 1158
Jungman G., Kamionkowski M., Griest K., 1996, PhR, 267, 195
Kang X., Macciò A. V., Dutton A. A., 2013, ApJ, 767, 22
Kawasaki M., Sugiyama N., Yanagida T., 1997, MPLA, 12, 1275

Klypin A., Kravtsov A. V., Valenzuela O., Prada F., 1999, ApJ, 522, 82
Kudoh H., Taruya A., Hiramatsu T., Himemoto Y., 2006, PhRvD, 73, 064006
Kuhlen M., Faucher-Giguère C.-A., 2012, MNRAS, 423, 862
Kusenko A., 2009, PhR, 481, 1
Lange A. E., et al., 2001, PhRvD, 63, 042001
Lapi A., Danese L., 2015, JCAP, 9, 003
Larson D., et al., 2011, ApJS, 192, 16
Lovell M. R., Frenk C. S., Eke V. R., Jenkins A., Gao L., Theuns T., 2014, MNRAS, 439, 300
Madau P., Rees M. J., 2001, ApJ, 551, L27
Madau P., Dickinson M., 2014, ARA&A, 52, 415
Mandelbaum R., Seljak U., Kauffmann G., Hirata C. M., Brinkmann J., 2006, MNRAS, 368, 715
Marassi S., Schneider R., Ferrari V., 2009, MNRAS, 398, 293
Mashchenko S., Couchman H. M. P., Wadsley J., 2006, Natur, 442, 539
McGreer I. D., Mesinger A., D'Odorico V., 2015, MNRAS, 447, 499
Menci N., Fiore F., Lamastra A., 2012, MNRAS, 421, 2384
Moore B., Ghigna S., Governato F., Lake G., Quinn T., Stadel J., Tozzi P., 1999, ApJ, 524, L19
Moster B. P., Naab T., White S. D. M., 2013, MNRAS, 428, 3121
Nakamura F., Umemura M., 2001, ApJ, 548, 19
Navarro J. F., Frenk C. S., White S. D. M., 1997, ApJ, 490, 493
Ostriker J. P., Gnedin N. Y., 1996, ApJ, 472, L63
Ott C. D., et al., 2013, ApJ, 768, 115
Pacucci F., Mesinger A., Haiman Z., 2013, MNRAS, 435, L53
Pagel B. E. J., 2000, PhR, 333, 433
Papastergis E., Martin A. M., Giovanelli R., Haynes M. P., 2011, ApJ, 739, 38
Pawlik A. H., Schaye J., van Scherpenzeel E., 2009, MNRAS, 394, 1812
Pereira E. S., Miranda O. D., 2010, MNRAS, 401, 1924
Phinney E. S., 2001, astro, arXiv:astro-ph/0108028
Planck Collaboration, et al., 2014, A&A, 571, A16
Planck Collaboration, et al., 2015, arXiv, arXiv:1502.01589
Pentericci L., et al., 2014, ApJ, 793, 113
Pontzen A., Governato F., 2014, Natur, 506, 171
Press W. H., Schechter P., 1974, ApJ, 187, 425
Reed D. S., Bower R., Frenk C. S., Jenkins A., Theuns T., 2007, MNRAS, 374, 2
Regimbau T., de Freitas Pacheco J. A., 2006, ApJ, 642, 455
Robertson B. E., et al., 2013, ApJ, 768, 71
Robertson B. E., Ellis R. S., Furlanetto S. R., Dunlop J. S., 2015, ApJ, 802, L19

Salpeter E. E., 1955, ApJ, 121, 161
Salucci P., Wilkinson M. I., Walker M. G., Gilmore G. F., Grebel E. K., Koch A., Frigerio Martins C., Wyse R. F. G., 2012, MNRAS, 420, 2034
Sandick P., Olive K. A., Daigne F., Vangioni E., 2006, PhRvD, 73, 104024
Sathyaprakash B. S., Schutz B. F., 2009, LRR, 12,
Scalo J. M., 1986, FCPh, 11, 1
Schenker M. A., Ellis R. S., Konidaris N. P., Stark D. P., 2014, ApJ, 795, 20
Schmidt M., 1963, ApJ, 137, 758
Schmidt M., 1959, ApJ, 129, 243
Schultz C., Oñorbe J., Abazajian K. N., Bullock J. S., 2014, MNRAS, 442, 1597
Scully S., Cassé M., Olive K. A., Vangioni-Flam E., 1997, ApJ, 476, 521
Shankar F., Lapi A., Salucci P., De Zotti G., Danese L., 2006, ApJ, 643, 14
Shaposhnikov M., Tkachev I., 2006, PhLB, 639, 414
Sheth R. K., Tormen G., 1999, MNRAS, 308, 119
Shull J. M., Harness A., Trenti M., Smith B. D., 2012, ApJ, 747, 100
Siana B., et al., 2010, ApJ, 723, 241
Slosar A., et al., 2013, JCAP, 4, 026
Spergel D. N., Steinhardt P. J., 2000, PhRvL, 84, 3760
Su K.-Y., Chen P., 2011, JCAP, 8, 016
Subramanian K., Cen R., Ostriker J. P., 2000, ApJ, 538, 528
Suwa Y., Takiwaki T., Kotake K., Sato K., 2007, ApJ, 665, L43
Tegmark M., et al., 2006, PhRvD, 74, 123507
Tegmark M., Silk J., Rees M. J., Blanchard A., Abel T., Palla F., 1997, ApJ, 474, 1
The Fermi LAT collaboration, 2015, JCAP, 9, 008
Thrane E., Romano J. D., 2013, PhRvD, 88, 124032
Thorne K. S., 1987, thyg.book, 330
Tonini C., Lapi A., Salucci P., 2006, ApJ, 649, 591
Treu T., Schmidt K. B., Trenti M., Bradley L. D., Stiavelli M., 2013, ApJ, 775, L29
Velander M., et al., 2014, MNRAS, 437, 2111
Viel M., Becker G. D., Bolton J. S., Haehnelt M. G., 2013, PhRvD, 88, 043502
Wang, F. Y., 2013, A&A, 556, A90
Wei J.-J., Hao J.-M., Wu X.-F., Yuan Y.-F., 2016, JHEAp, 9, 1
Weinberg M. D., Katz N., 2002, ApJ, 580, 627
Yang Y. P., Wang F. Y., Dai Z. G., 2015, A&A, 582, A7
Zhou B., Liang Y.-F., Huang X., Li X., Fan Y.-Z., Feng L., Chang J., 2015, PhRvD, 91, 123010

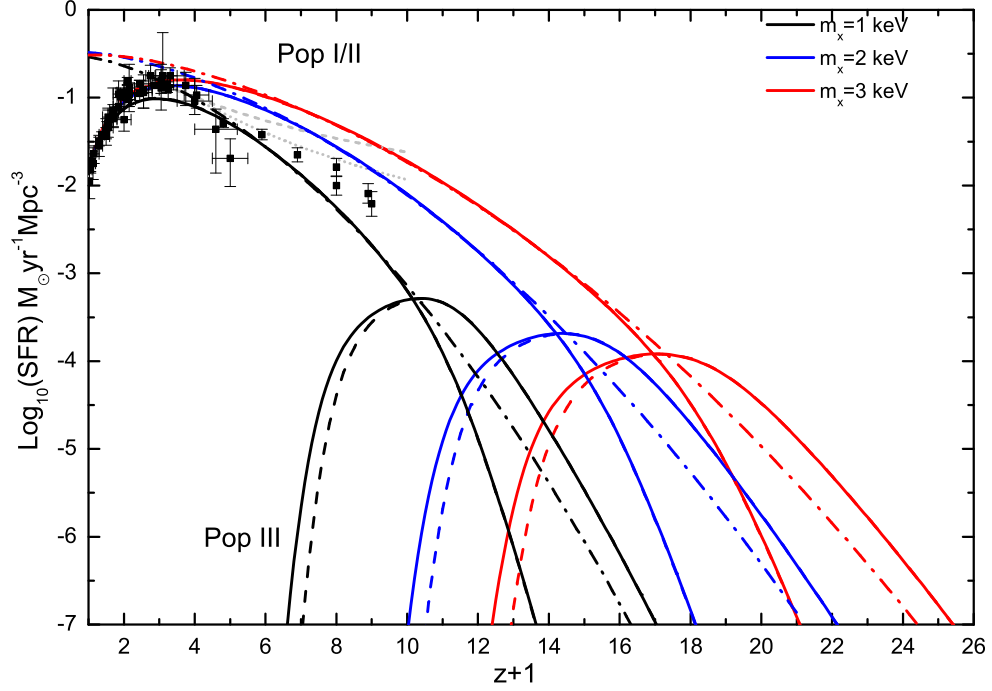Fɪɢ. 1.— SFRs for Pop I/II and Pop III stars with different WDM particle masses (from bottom to top): $m_x = 1\,\mathrm{keV}$ (black lines), $m_x = 2\,\mathrm{keV}$ (blue lines), $m_x = 3\,\mathrm{keV}$ (red lines). The solid lines correspond to the SIMF and the dashed lines correspond to the CIMF. The gray dashed and dotted lines are the SFRs taken from Robertson et al. (2015). The dash-dotted lines are the SFRs calculated by the relation of SFR$\propto M_h^{0.9}$ in a structure. The observation data is taken from Madau & Dickinson (2014), which includes the measurements from far-ultraviolet and infrared luminosity functions of galaxies.
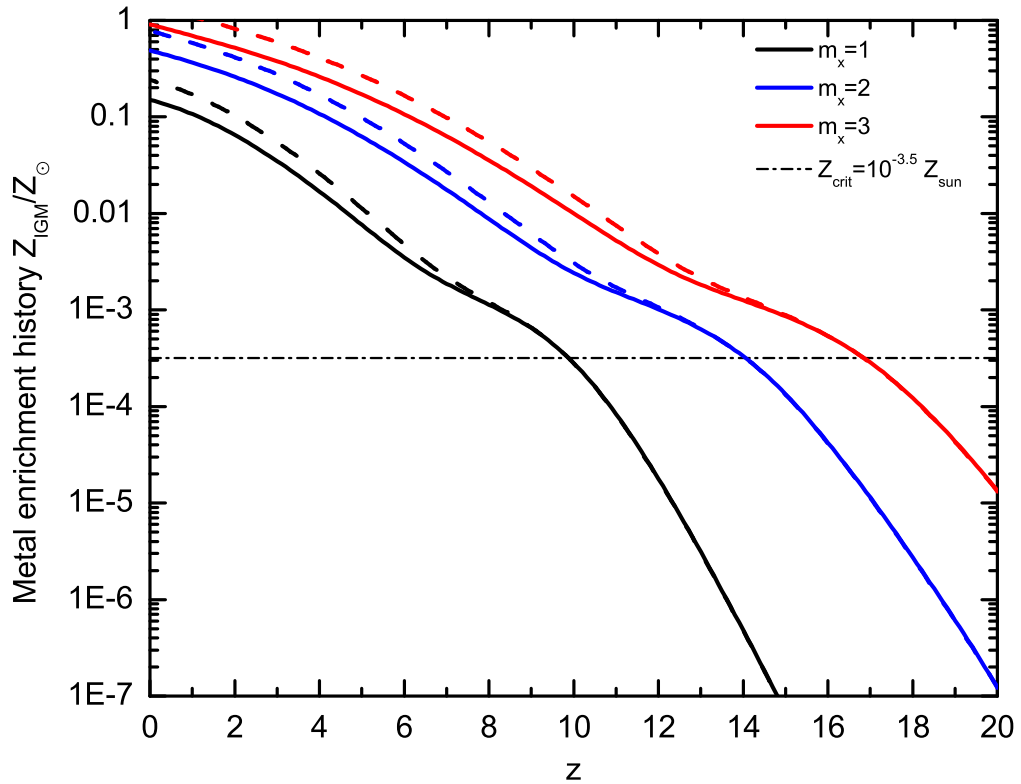

Fɪɢ. 2.— The metal enrichment history of the IGM correspond to the SFRs in Figure 1. The solid lines correspond to SIMF, and the dashed lines correspond to CIMF. The dash-dotted line corresponds to the critical metallicity of $Z = 10^{3.5}Z_\odot$.
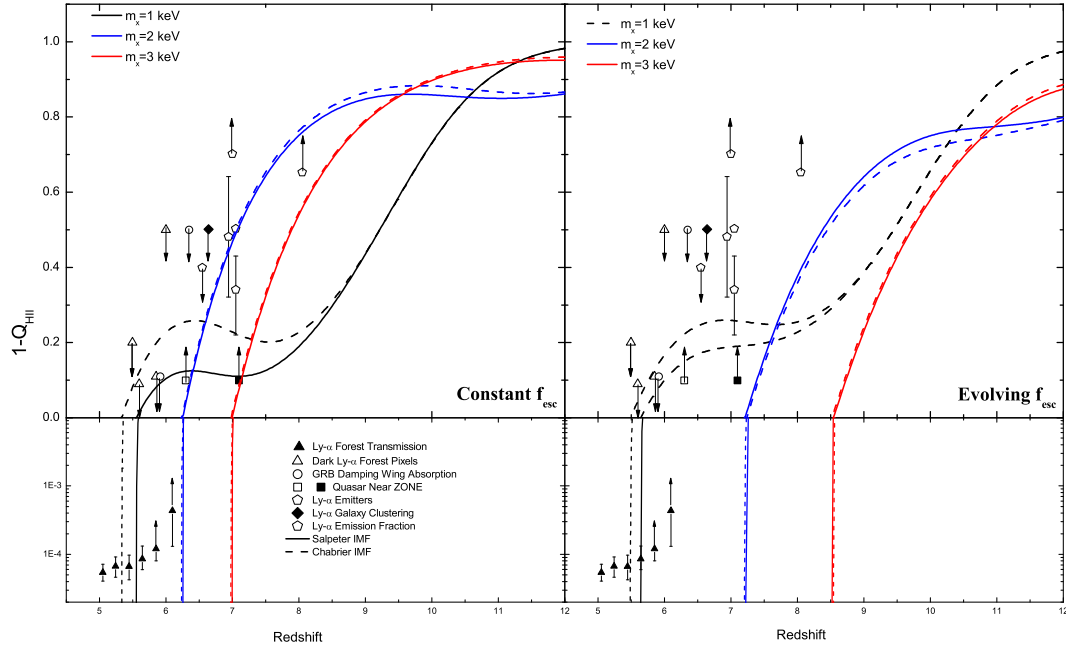
FIG. 3.— The corresponding neutral fraction of $1 - Q_{H_{II}}$ for the SFRs given in Figure 1. Left: The neutral fractions derived by assuming a constant f_{esc}. Right: The neutral fractions derived by assuming an evolving f_{esc} of equation (28). Measurements of IGM neutral fractions are derived from Lyα emitting galaxies (Pentericci et al. 2014; Schenker et al. 2014), constraints from the Lyα of GRB host galaxies (Chornock et al. 2013), and inferences from dark pixels in Lyα forest measurement (McGreer, Mesinger, & D'Odorico 2015).
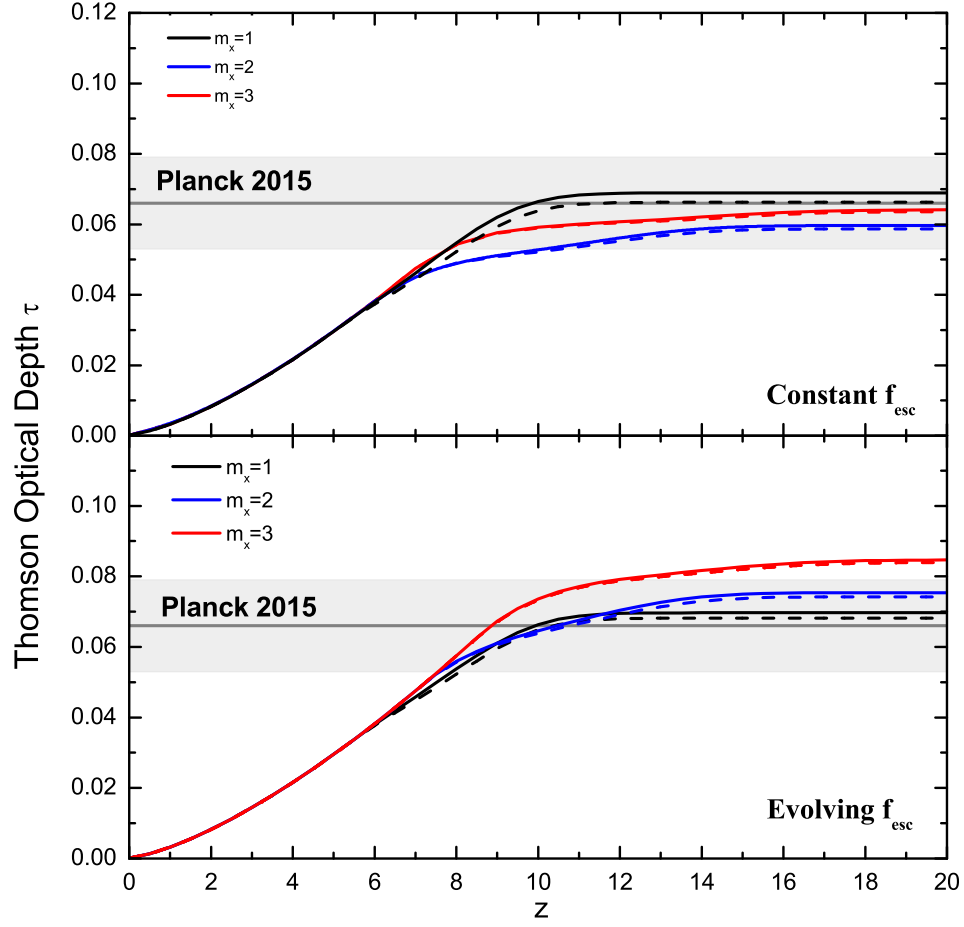
Fig. 4.— Top: The model-predicted CMB optical depth (τ) correspond to the reionization of the left panel of Figure 3, where a constant escape fraction is assumed. Bottom: The model-predicted CMB optical depth (τ) with an evolving escape fraction, which corresponds to the reionization of the right panel of Figure 3. The shade region is the CMB optical depth measured by *Planck* with $\tau = 0.066^{+0.013}_{-0.013}$.
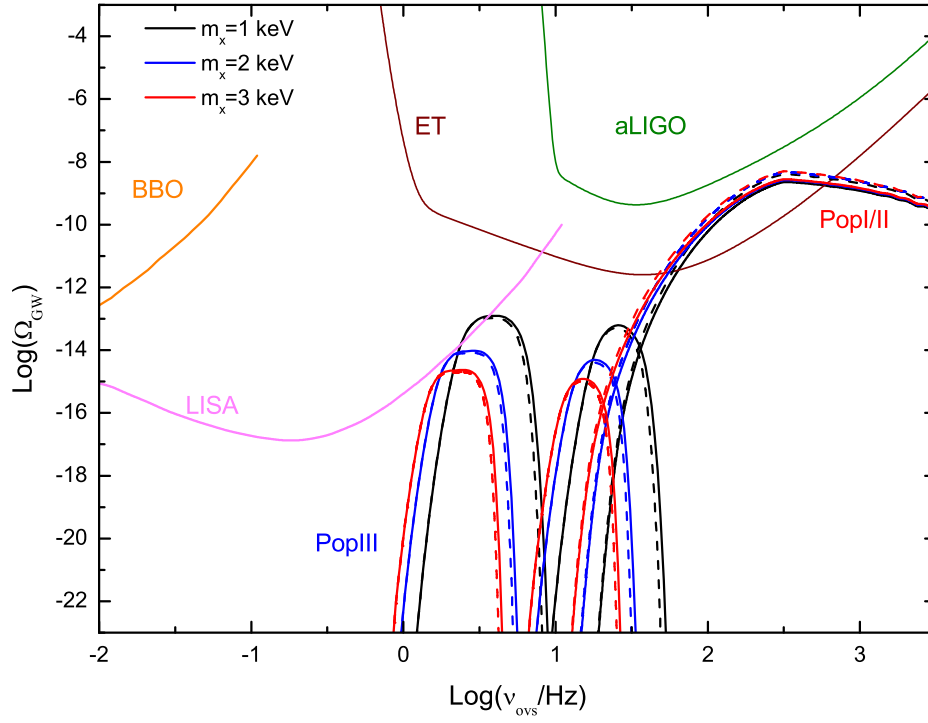
Fɪɢ. 5.— The stochastic gravitational wave background from Pop I/II and Pop III black holes, which correspond to the SFRs in Figure 1. The detection thresholds of advanced LIGO, ET, LISA, and BBO are labeled with different colors, where one year of observation is assumed.